View metadata, citation and similar papers at core.ac.uk
brought to you by CORE
provided by Springer - Publisher Connector

Appl Phys A (2012) 108:521–528
DOI 10.1007/s00339-012-6977-4

Applied Physics A
Materials Science & Processing

# An attempt to design long-wavelength (>2 μm) InP-based GaInNAs diode lasers

**Robert P. Sarzała · Łukasz Piskorski · Paweł Szczerbiak · Robert Kudrawiec · Włodzimierz Nakwaski**

Received: 8 February 2012 / Accepted: 5 May 2012 / Published online: 23 May 2012
© The Author(s) 2012. This article is published with open access at Springerlink.com

**Abstract** In the present paper, anticipated performance characteristics of various InP-based GaInNAs quantum-well (QW) active regions are determined with the aid of our comprehensive computer model for various sets of parameters (temperature, carrier concentration, QW thickness). It is evident from this analysis that the compressively strained InP-based $Ga_{0.12}In_{0.88}N_{0.02}As_{0.98}/Ga_{0.275}In_{0.725}As_{0.6}P_{0.4}$ QW structure may offer expected lasing emission. Its maximal optical gain of over 2150 $cm^{-1}$ has been determined at room temperature for the wavelength of about 2815 nm for the QW thickness of 10 nm and the carrier concentration of $5 \times 10^{18}$ $cm^{-3}$. Therefore, the above InP-based QW structure may be successfully applied in compact semiconductor laser sources of the desired radiation of wavelengths longer at room temperature than even 2800 nm. Similar GaAs-based devices emit radiation of distinctly shorter wavelengths, whereas GaSb-based ones avail themselves of more expensive substrates as well as exhibit lower thermal conductivities and worse carrier confinements.

## 1 Introduction

The mid-infrared (3.0–5.5 μm) spectral range enjoys currently an increasing interest of laser designers because of its potential wide applications in a distant air monitoring, laser spectroscopy, medical diagnostics, thermovision measurements, and wireless optical communication, to name the most important application areas. Semiconductor lasers emitting radiation of wavelengths longer than 2 μm are currently produced with the aid of the GaSb technology [1]; however, manufacturing of GaSb structures is relatively expensive and complex, thermal conductivities of GaSb-based semiconductors [2–5] are disappointedly low, carrier confinement in GaSb active regions [6, 7] is relatively low, and GaSb substrates [8] are still expensive and of limiting sizes. Therefore, there is a wide interest to replace in this application the GaSb-based lasers with the InP-based ones of well known, much simpler, and less expensive technology, provided that a proper active-region structure will be applied ensuring laser emission of the expected infrared wavelength range. It may be accomplished using some of the diluted nitrides as, for example, InNAs, GaInNAs, and GaInNAsSb. They are very special materials, because contrary to most of known semiconductors, an increase in their nitride contents leads to reductions of both the lattice constant and the energy gap. Their application enables reaching in the GaAs-based diode lasers both the 1.31-μm and the 1.55-μm bands [9] used in the fiber optical communication. With the aid of the InP-based technology, however, it is expected to reach even the 3.5 μm emission.

In this paper, possibility of designing the active region for InP-based quantum-well (QW) semiconductor laser emitting the 2.0–3.5 μm radiation with a diluted-nitride active region is considered.

## 2 Designing

Let us consider the structure grown on the InP substrate with the GaInNAs/GaInAsP quantum-well active region. Its ma-

R.P. Sarzała · Ł. Piskorski (✉) · P. Szczerbiak · W. Nakwaski
Photonics Group, Institute of Physics, Lodz University of Technology, Wolczanska 219, 90-924 Lodz, Poland
e-mail: lukasz.piskorski@p.lodz.pl
Fax: +48-42-6313639

P. Szczerbiak · R. Kudrawiec
Institute of Physics, Wroclaw University of Technology, Wybrzeze Wyspianskiego 27, 50-370 Wroclaw, Poland

**Table 1** Material parameters known for some binary $A^{III}B^{V}$ compounds. $a_{lc}$ (300 K)—room-temperature lattice constant, $T$—absolute temperature, $E_g$ (0 K)—energy gap at 0 K, $\alpha$ and $\beta$—Varshni parameters [14], $\Delta_{so}$—spin-orbit splitting, $m_e$, $m_{hh}$ and $m_{lh}$—electron, heavy-hole and light-hole effective mass, $m_0$—electron rest mass, $a_c$, $a_v$ and $b$—deformation potentials, $c_{11}$ and $c_{12}$—elastic constants

| Parameter | GaAs | InAs | GaN | InN | InP | GaP |
|---|---|---|---|---|---|---|
| $a_{lc}$ (300 K), (Å) | 5.65325 [10] | 6.0583 [10] | 4.50 [11] | 4.98 [11] | 5.8697 [10] | 5.4505 [10] |
| $da_{lc}/dT$ ($10^{-5}$ Å/K) | 3.88 [10] | 2.74 [10] | 2.05 [12] | 2.83 [12] | 2.79 [10] | 2.92 [10] |
| $E_g$ (0 K), (eV) | 1.519 [10] | 0.417 [10] | 3.299[a] [11] | 0.78[a] [11] | 1.4236 [10] | 2.8758[a,b] |
| $\alpha$ (meV/K) | 0.5405 [10] | 0.276 [10] | 0.593[a] [11] | 0.245[a] [11] | 0.363 [10] | 0.96[a,b] |
| $\beta$ (K) | 204 [10] | 93 [10] | 600[a] [11] | 624[a] [11] | 162 [10] | 423[a,b] |
| $\Delta_{so}$ (eV) | 0.341 [10] | 0.39 [10] | 0.017 [11] | 0.005 [11] | 0.108[a] [10] | 0.08[a] [10] |
| $m_e$ ($m_0$) | 0.067 [13] | 0.024 [13] | 0.15[a] [13] | 0.03[a] [13] | 0.07927 [13] | 0.114[a] [13] |
| $m_{hh}$ ($m_0$) | 0.33 [13] | 0.26 [13] | 0.83 [13] | 1.261 [13] | 0.46 [13] | 0.34[a] [13] |
| $m_{lh}$ ($m_0$) | 0.090 [13] | 0.027 [13] | 0.22 [13] | 0.100 [13] | 0.12 [13] | 0.20[a] [13] |
| $a_c$ (eV) | −7.17 [10] | −5.08 [10] | −6.71 [11] | −2.65 [11] | −6.0[a] [10] | −8.2[a] [10] |
| $a_v$ (eV) | 1.16 [10] | 1.00 [10] | 0.69 [11] | 0.7 [11] | 0.6[a] [10] | 1.7[a] [10] |
| $b$ (eV) | −2.0 [10] | −1.8 [10] | −2.0 [11] | −1.2 [11] | −2.0[a] [10] | −1.6[a] [10] |
| $c_{11}$ (GPa) | 122.1 [10] | 83.29 [10] | 293 [11] | 187 [11] | 101.1[a] [10] | 140.5[a] [10] |
| $c_{12}$ (GPa) | 56.6 [10] | 45.26 [10] | 159 [11] | 125 [11] | 56.1[a] [10] | 62.03[a] [10] |

[a]Values included for information only to complete the table and not used in the calculations

[b]Values proposed by authors of this paper leading to results, which for temperatures higher than 90 K, are in a very good agreement with the relation $E_g(T) = 2.886 + 0.1081\,[1 - \coth(164/T)]$ recommended in [10]

**Table 2** Nonzero bowing parameters of the GaInAs ternary compound. $E_g$—energy gap, $\Delta_{so}$—spin-orbit splitting, $m_e$—electron effective mass, $m_0$—electron rest mass, $a_c$—deformation potential

| Bowing parameter for | GaInAs |
|---|---|
| $E_g$ (eV) | 0.477 [10] |
| $\Delta_{so}$ (eV) | 0.15 [10] |
| $m_e$ ($m_0$) | 0.008 [13] |
| $a_c$ (eV) | 2.61 [10] |

terial parameters are mostly found with the aid of interpolations between values known for binary compounds (Table 1). Four bowing parameters used to obtain band parameters for GaInAs are listed in Table 2. It has been found [10] that for some lattice-matched quaternary materials, quite exact results may be reached with the aid of the interpolation between values known for two lattice-matched materials, from among at least one should be a ternary material. Hence, in the case of GaInAsP, we are using linear interpolations between values of parameters known for InP and the lattice-matched $Ga_{0.47}In_{0.53}As$ with one exception: for an energy-gap determination we are using the interpolation between all four binary values with the nonlinear parameter equal to 0.13 eV [10].

The energy gap in $Ga_{1-x}In_xN_yAs_{1-y}$, on the other hand, may be found from [15]:

$$E_g^{GaInNAs} = (1-x)E_g^{GaNAs} + xE_g^{InNAs} - x(1-x)C \qquad (1)$$

with

$$E_g^{GaNAs} = \frac{1}{2}\Big[E_N^{GaNAs} + E_g^{GaAs} - \sqrt{\left(E_N^{GaNAs} - E_g^{GaAs}\right)^2 + 4\left(V^{GaNAs}\right)^2 y}\Big], \qquad (2)$$

$$E_g^{InNAs} = \frac{1}{2}\Big[E_N^{InNAs} + E_g^{InAs} - \sqrt{\left(E_N^{InNAs} - E_g^{InAs}\right)^2 + 4\left(V^{InNAs}\right)^2 y}\Big] \qquad (3)$$

with: $E_N^{GaNAs} = 1.65$ eV, $E_N^{InNAs} = 1.44$ eV, $V^{GaNAs} = 2.7$ eV, $V^{InNAs} = 2.0$ eV [11] and $C = 0.477$ eV [10].

Taking into account published experimental values of the electron effective mass $m_e^{GaInNAs}$ in $Ga_{1-x}In_xN_yAs_{1-y}$ (Fig. 1), we propose the following simple approximate relation to calculate this parameter:

$$m_e^{GaInNAs} = m_e^{Ga_{1-x}In_xAs} + 0.032m_0 \qquad (4)$$

The above electron effective mass $m_e^{GaInNAs}$ is assumed to depend on the indium contents $x$ only whereas its dependence on the analogous nitrogen contents $y$ is taken into account with the aid of the constant $0.032m_0$ term added to the effective mass determined for GaInAs (see Fig. 1).

For remaining parameters, their $Q$ values in the GaInNAs quaternary material can be expressed as a weighted sum of the related $T$ values known for ternary compounds [28]:

$$Q^{\mathrm{GaInNAs}} = \frac{x(1-x)[yT^{\mathrm{GaInN}} + (1-y)T^{\mathrm{GaInAs}}] + y(1-y)[xT^{\mathrm{InNAs}} + (1-x)T^{\mathrm{GaNAs}}]}{x(1-x) + y(1-y)} \quad (5)$$

where those $T$ values are expressed with the aid of related $B$ values known for the binary compounds and $C$-corresponding bowing parameters:

$$T^{\mathrm{GaInN}} = (1-x)B^{\mathrm{GaN}} + xB^{\mathrm{InN}} - (1-x)xC^{\mathrm{GaInN}}, \quad (6a)$$

$$T^{\mathrm{GaInAs}} = (1-x)B^{\mathrm{GaAs}} + xB^{\mathrm{InAs}} - (1-x)xC^{\mathrm{GaInAs}}, \quad (6b)$$

$$T^{\mathrm{InNAs}} = yB^{\mathrm{InN}} + (1-y)B^{\mathrm{InAs}} - y(1-y)C^{\mathrm{InNAs}}, \quad (6c)$$

$$T^{\mathrm{GaNAs}} = yB^{\mathrm{GaN}} + (1-y)B^{\mathrm{GaAs}} - y(1-y)C^{\mathrm{GaNAs}} \quad (6d)$$

If all the bowing $C$ parameters are equal to zero for a given band parameter, Eq. (5) reduces to (7):

$$Q^{\mathrm{GaInNAs}} = (1-x)yB^{\mathrm{GaN}} + (1-x)(1-y)B^{\mathrm{GaAs}} + xyB^{\mathrm{InN}} + x(1-y)B^{\mathrm{InAs}} \quad (7)$$

When the layer of lattice constant $a_{\mathrm{lc}}^{\mathrm{QW}}$ is grown on the substrate of somewhat different lattice constant $a_{\mathrm{lc}}^{\mathrm{sub}}$, this lattice mismatch may be accommodated providing the layer is thinner than its critical thickness $h_{\mathrm{c}}$ [13]:

$$h_{\mathrm{c}} = 0.1\left(\frac{16}{|\varepsilon|}\right)^{2.4} \quad (8)$$

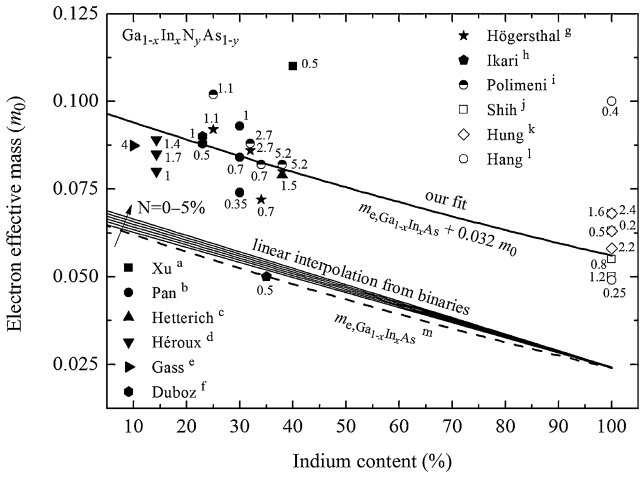


**Fig. 1** Electron effective mass vs. indium content for as-grown GaInNAs. Thin solid lines correspond to the linear interpolation between effective masses in binary materials; dashed line is plotted for the electron effective mass in GaInAs, whereas the thick solid line is our fit. Experimental points present values of N content in GaInNAs. [a]See [16]. [b]See [17]. [c]See [18]. [d]See [19]. [e]See [20]. [f]See [21]. [g]See [22]. [h]See [23]. [i]See [24]. [j]See [25]. [k]See [26]. [l]See [27]. [m]See [13]

where the critical thickness $h_{\mathrm{c}}$ is given in nm and strains $\varepsilon$ are determined in % with the aid of

$$\varepsilon = \frac{a_{\mathrm{lc}}^{\mathrm{sub}} - a_{\mathrm{lc}}^{\mathrm{QW}}}{a_{\mathrm{lc}}^{\mathrm{QW}}} \quad (9)$$

As expected, the critical thickness $h_{\mathrm{c}}$ is monolithically being reduced with an increase in strain $\varepsilon$ (Fig. 2). Temperature dependence of lattice constants may be given by the following simple relation:

$$a_{\mathrm{lc}}(T) = a_{\mathrm{lc}}(300\ \mathrm{K}) + \frac{\mathrm{d}a_{\mathrm{lc}}}{\mathrm{d}T}(T - 300\ \mathrm{K}) \quad (10)$$

where, for a given quaternary material, values of the lattice constant $a_{\mathrm{lc}}$ and its temperature derivative are determined as a linear interpolation (7) between their values known for all four binary compounds (Table 1). Temperature dependence of energy gaps of binary compounds is given by [14]:

$$E_{\mathrm{g}}(T) = E_{\mathrm{g}}(0\ \mathrm{K}) - \frac{\alpha T^2}{T + \beta} \quad (11)$$

where $\alpha$ and $\beta$ are given in Table 1.

According to the BAC model [29], adding of nitrogen to $Ga_{1-x}In_xAs$ results only in shifting down the conduction band, whereas discontinuity of the valence band edge changes much less. Therefore, the $\Delta E_{\mathrm{v}}$ discontinuity of the valence-band edge between the lattice-matched GaInAsP and $Ga_{1-x}In_xN_yAs_{1-y}$ has been assumed to be the same as its value for the lattice-matched GaInAsP and $Ga_{1-x}In_xAs$.

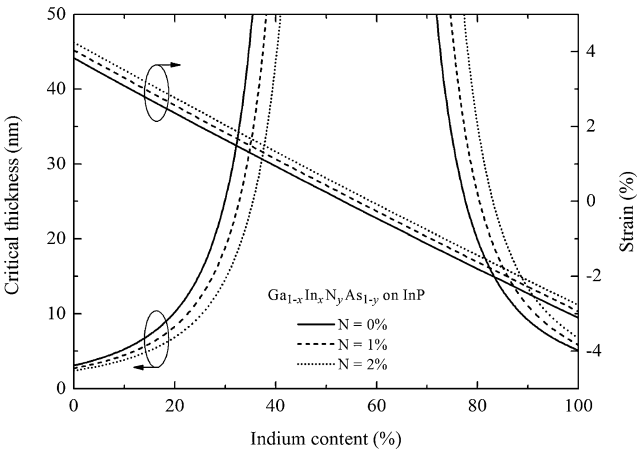


**Fig. 2** Calculated critical thickness and strain in the $Ga_{1-x}In_xN_yAs_{1-y}$ QW grown on the InP substrate for its (001) growth orientation versus the In content $x$ plotted for various N contents $y$

For strained layers, we are using approach of Pikus and Bir [30, 31] in a form given by Chuang [32]. Then, in the strained semiconductor, the conduction $E_c^{str}$ and the valence $E_v^{str}$ band edges, respectively, are related to their $E_c$ and $E_v$ values in the unstrained material in the following way:

$$\Delta E_c^{str} = E_c + \Delta E_c^{hy}, \tag{12}$$

$$\Delta E_v^{str} = E_v + \Delta E_v^{hy} \tag{13}$$

where

$$\Delta E_c^{hy} = 2a_c\left(1 - \frac{c_{12}}{c_{11}}\right)\varepsilon, \tag{14}$$

$$\Delta E_v^{hy} = 2a_v\left(1 - \frac{c_{12}}{c_{11}}\right)\varepsilon \tag{15}$$

Values of elastic constants $c_{11}$ and $c_{12}$ and deformation potentials $a_c$ and $a_v$ are listed in Table 1. Similarly, heavy- and light-hole energies may be found from

$$E_{hh}^{str} = E_v^{str} + \Delta E_{hh}^{sh}, \tag{16}$$

$$E_{lh}^{str} = E_v^{str} + \Delta E_{lh}^{sh} \tag{17}$$

where

$$\Delta E_{hh}^{sh} = -\frac{1}{2}\Delta E^{sh}, \tag{18}$$

$$\Delta E_{lh}^{sh} = -\frac{1}{2}\Delta_{so} + \frac{1}{4}\Delta E^{sh} + \frac{1}{2}\sqrt{\Delta_{so}^2 + \Delta_{so}\Delta E^{sh} + \frac{9}{4}\left(\Delta E^{sh}\right)^2} \tag{19}$$

with

$$\Delta E^{sh} = -2b\left(1 + 2\frac{c_{12}}{c_{11}}\right)\varepsilon \tag{20}$$

where the spin-orbit splitting $\Delta_{so}$ and the $a_c$, $a_v$, and $b$ deformation potentials are given in Table 1.

Generally, during a mismatch growth of relatively thin semiconductor layers, strain is accommodated changing some semiconductor properties (for example, its energy gap), which may be intentionally used (bandgap engineering). Growth of too thick mismatch layers, on the other hand, may result in their cracking.

## 3 Optical gain

Assuming parabolic band-gap approximation, the optical gain spectra within the quantum well are determined with the aid of the Fermi's golden rule [32]:

$$g(\hbar\omega) = \sum_i \int_{-\infty}^{\infty} g_i(E)\Lambda(\hbar\omega - E)\,\mathrm{d}E \tag{21}$$

where $i$ denotes number of available level pairs and

$$g_i(\hbar\omega) = \frac{e^2\pi\hbar}{n_R c m_0^2 \varepsilon_0}\frac{M^2\rho_r^{2D}(\hbar\omega)}{\hbar\omega} \times \left\{f_c\left[E_e(i,\hbar\omega)\right] - f_v\left[E_h(i,\hbar\omega)\right]\right\} \tag{22}$$

In the above relations, $e$ stands for the electron charge, $n_R$ is the index of refraction, $c$ is the speed of light in vacuum, $m_0$ is the rest electron mass, $\varepsilon_0$ is the vacuum dielectric constant, $M$ stands for the momentum matrix element, $\rho_r^{2D}$ is the two-dimensional reduced density of states, $f_c$ and $f_v$ stand for the Fermi–Dirac functions determined for electrons in the conduction band and holes in the valence band, respectively, $E_e$ and $E_h$ are the energies of the recombining electron and hole, respectively, and $\Lambda$ is the broadening function [33], usually of Lorentzian type.

## 4 Gain spectra

The optimal active-region structure is expected to ensure low-threshold room-temperature emission of the radiation of the desired wavelength, this time—the radiation of the wavelength longer than 2 μm. Performance of the QW laser depends mostly on its QW structure, which means—on compositions and thickness of its layers. In this section, an impact of parameters of the QW InP-based GaInNAs laser structure (including intentionally introduced strain) on a laser performance will be considered leading to a determination of an optimal QW active-region structure for the laser emitting the desired radiation.

At first, let us consider the unstrained ($\varepsilon = 0$) single quantum well (SQW) $Ga_{0.44}In_{0.56}N_{0.01}As_{0.99}/Ga_{0.275}In_{0.725}As_{0.6}P_{0.4}$ active-region InP-based device at room temperature ($T = 300$ K). Its band structure determined with the aid of the model presented in previous sections is shown in Fig. 3a for the quantum-well width $d_{QW} = 6$ nm. Electron and hole energy QW states as well as depths of successive potential barriers are indicated. As one can see, two electron states as well as three heavy-hole states and one light-hole state are confined within the QW, although both the (e2) state within the conduction-band QW and the (hh3) state within the analogous valence-band QW are only partly confined. The transition between the first QW electron (e1) and hole (hh1) states corresponds to the wavelength of about 1800 nm. This wavelength is much longer than possible wavelengths for analogous transitions between QW states in similar lasers grown on GaAs [9], which may enable manufacturing efficient laser sources emitting such a long-wavelength radiation.

Corresponding gain spectra determined for the same QW active region structure but for three various carrier concentrations $n$ and three ambient temperatures $T$ are plotted in

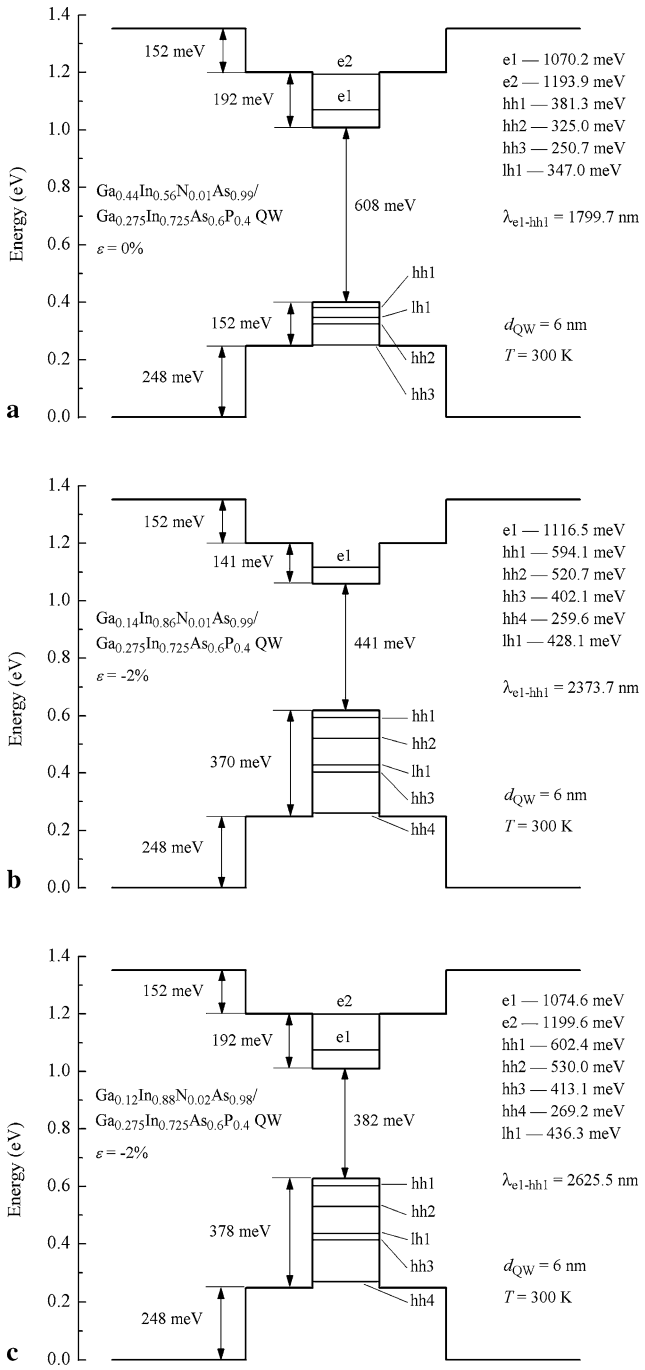


**Fig. 3** Band structures of the as-grown unstrained 6-nm $Ga_{1-x}In_xN_yAs_{1-y}/Ga_{0.275}In_{0.725}As_{0.6}P_{0.4}$ QWs. The wavelengths $\lambda_{e1\text{-}hh1}$ determined for the transitions between the first electron and heavy-hole levels are shown. (**a**) $x = 56$ %, $y = 1$ %. (**b**) $x = 86$ %, $y = 1$ %. (**c**) $x = 88$ %, $y = 2$ %

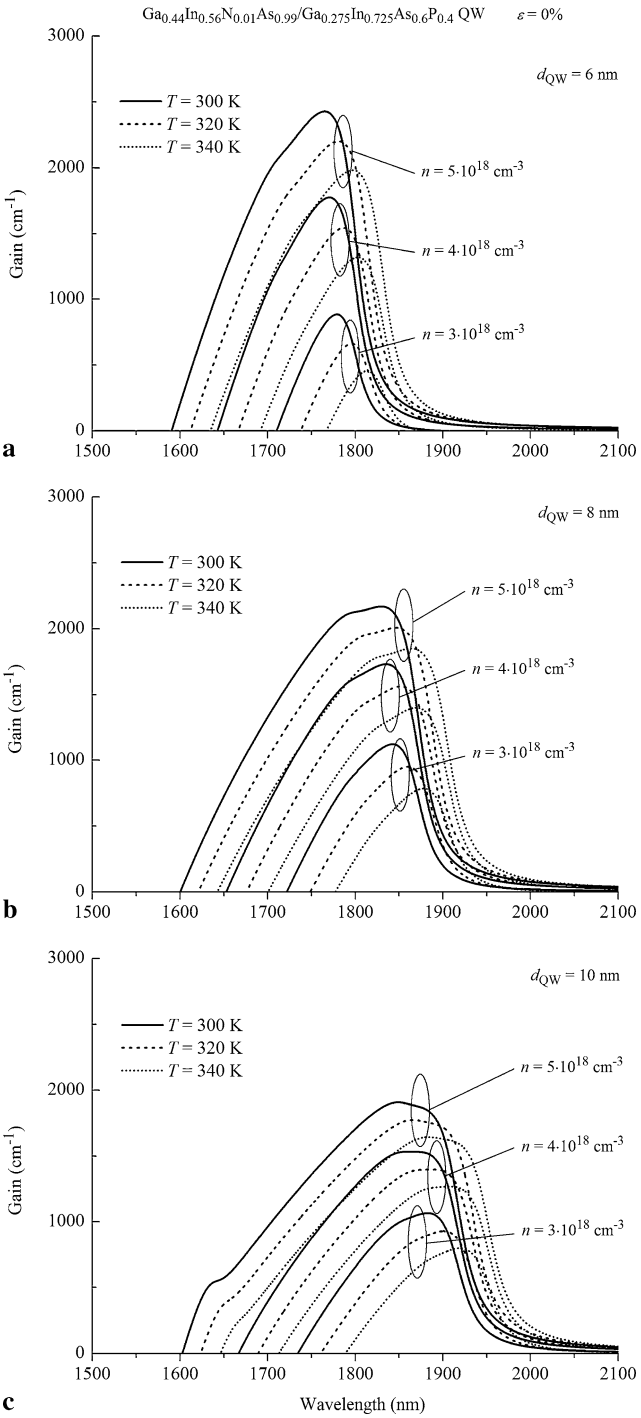


**Fig. 4** Gain spectra of the as-grown unstrained $Ga_{0.44}In_{0.56}N_{0.01}As_{0.99}/Ga_{0.275}In_{0.725}As_{0.6}P_{0.4}$ QW determined for various both the ambient temperatures $T$ and the active-region electron concentrations $n$. (**a**) $d_{QW} = 6$ nm. (**b**) $d_{QW} = 8$ nm. (**c**) $d_{QW} = 10$ nm

Fig. 4a. As expected, increases in the active-region temperature and in the active-region carrier concentration are followed by red shifts of the whole gain spectrum and the optical gain, respectively. For the room ambient temperature, positive optical gain is available in this QW for wavelength values larger than about 1710 nm for $n = 3 \times 10^{18}$ cm$^{-3}$, larger than about 1642 nm for $n = 4 \times 10^{18}$ cm$^{-3}$, and larger than about 1590 nm for $n = 5 \times 10^{18}$ cm$^{-3}$. Maximal optical gain of about 883 cm$^{-1}$ has been determined for about 1779 nm, of about 1774 cm$^{-1}$ for about 1770 nm, and of

about 2428 cm$^{-1}$ for about 1765 nm for the above three corresponding carrier concentrations.

An increase in the quantum-well width $d_{QW}$ results in a considerable increase in the above wavelength values. Figures 4b and 4c present analogous to Fig. 4a gain spectra for lasers with unstrained 8-nm and 10-nm, respectively, QW widths. As one can see, for the room ambient temperature and the carrier concentration of $5 \times 10^{18}$ cm$^{-3}$, maximal optical gain corresponds to the wavelength of about 1765 nm for $d_{QW} = 6$ nm, whereas it is shifted to about 1830 nm for $d_{QW} = 8$ nm and to about 1849 nm for $d_{QW} = 10$ nm.

An additional red shift of gain spectra may be expected in compressively strained active regions. Figure 3b presents band structure of such a $Ga_{0.14}In_{0.86}N_{0.01}As_{0.99}/Ga_{0.275}In_{0.725}As_{0.6}P_{0.4}$ QW ($\varepsilon = -2$ %). As one can see, only one electron state may be confined within the relatively shallow conduction-band QW whereas the much deeper valence-band QW ensures distinctly better hole confinements. This time an energy distance between the first electron and heavy-hole levels corresponds to the wavelength of about 2374 nm, much longer than that in the analogous unstrained QW (cf. Fig. 3a). Room-temperature gain spectra determined for this QW structure with the same as the above QW widths of 6 nm, 8 nm and 10 nm are plotted in Figs. 5a, 5b, and 5c, respectively. As compared with analogous spectra plotted in Fig. 4 for the unstrained QW, the spectra determined for the above compressively strained QW are distinctly red shifted. The maximal optical gain of about 2176 cm$^{-1}$ determined for the wavelength of about 2501 nm for the above compressively strained 10-nm QW for the room temperature and the active-region carrier concentration of $5 \times 10^{18}$ cm$^{-3}$ is distinctly red shifted as compared with the maximal optical gain at 1849 nm determined for the analogous unstrained QW (cf. Fig. 4c).

Let us consider further optimization of the QW structure testing an impact of the nitrogen mole fraction in its active-region material increased to 2 %. The band structure of such a $Ga_{0.12}In_{0.88}N_{0.02}As_{0.98}/Ga_{0.275}In_{0.725}As_{0.6}P_{0.4}$ QW is plotted in Fig. 3c. As one can see, four hole energy states are strongly confined within the valence band QW. This time the energy distance between the first electron and hole QW states corresponds to as long transition wavelength as about 2626 nm, much longer than that in the previous QW structure (Fig. 3b). Successive figures, i.e., Figs. 6a, 6b, and 6c, present room-temperature gain spectra determined for the above structure and for three values of thickness $d_{QW} = 6$ nm, 8 nm and 10 nm, respectively, of its QW. It is evident that an increase in the nitrogen mole fraction leads to a considerable shift of the compressively strained QW gain spectra towards longer wavelengths. For the considered QW structure and the same as previously both the QW thickness of 10 nm and the carrier concentration of $5 \times 10^{18}$ cm$^{-3}$, maximal optical gain is at room temperature shifted as much

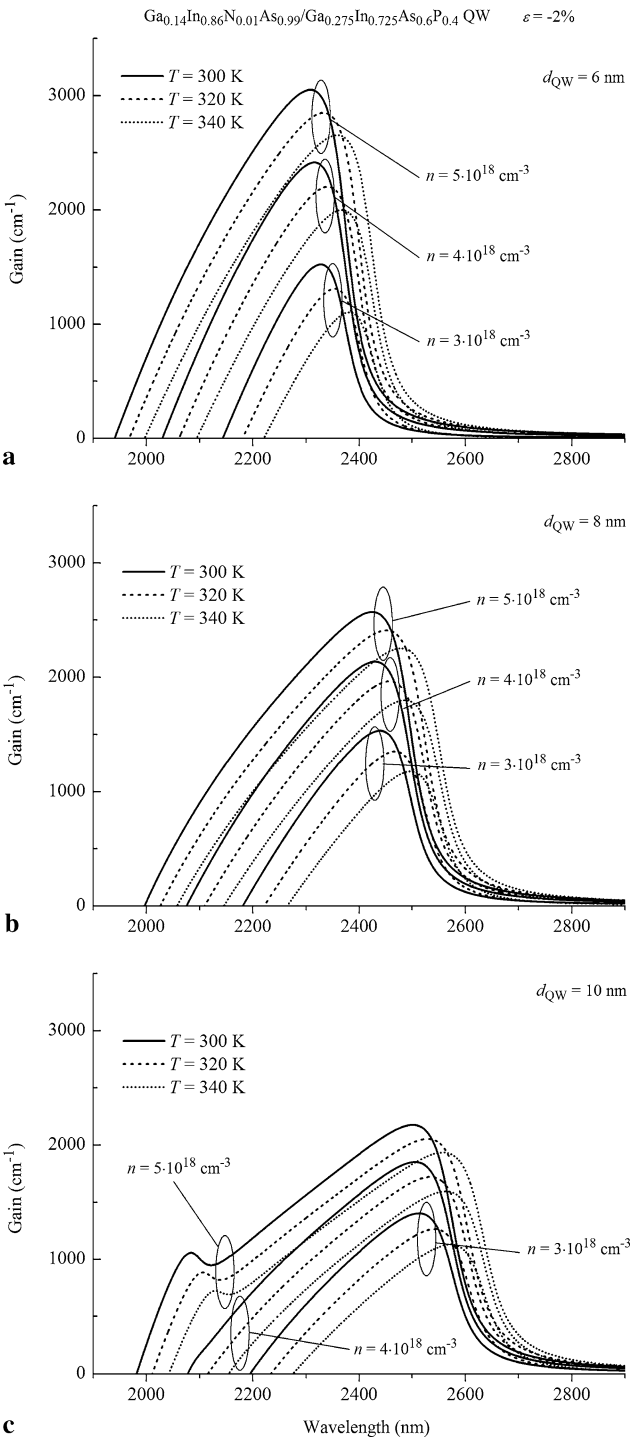


**Fig. 5** Gain spectra of the as-grown compressively strained ($\varepsilon = -2$ %) $Ga_{0.14}In_{0.86}N_{0.01}As_{0.99}/Ga_{0.275}In_{0.725}As_{0.6}P_{0.4}$ QW determined for various both the ambient temperatures $T$ and the active-region electron concentrations $n$. (**a**) $d_{QW} = 6$ nm. (**b**) $d_{QW} = 8$ nm. (**c**) $d_{QW} = 10$ nm

as to about 2815 nm. For thinner QWs, i.e., for $d_{QW} = 6$ nm and 8 nm, and the same carrier concentration, the above maximal optical gain corresponds to about 2546 nm and to about 2706 nm, respectively. The above values confirm our

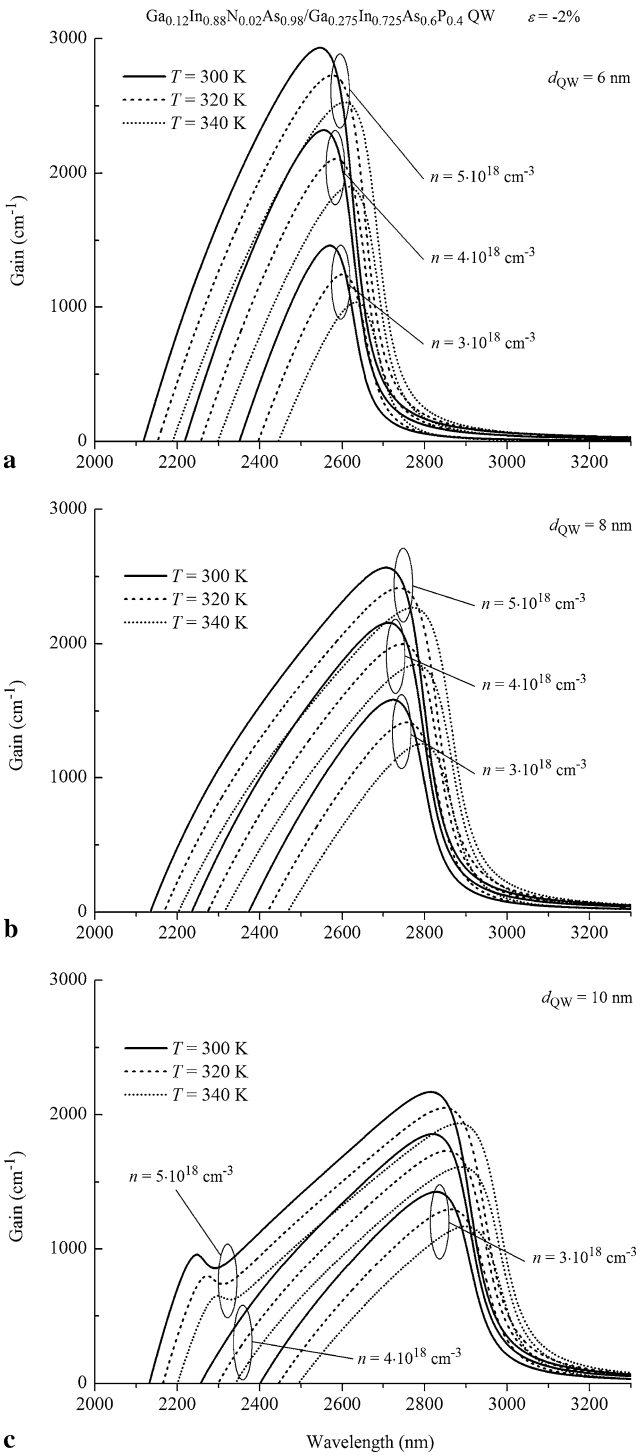


**Fig. 6** Gain spectra of the as-grown compressively strained ($\varepsilon = -2$ %) $Ga_{0.12}In_{0.88}N_{0.02}As_{0.98}/Ga_{0.275}In_{0.725}As_{0.6}P_{0.4}$ QW determined for various both the ambient temperatures $T$ and the active-region electron concentrations $n$. (**a**) $d_{QW} = 6$ nm. (**b**) $d_{QW} = 8$ nm. (**c**) $d_{QW} = 10$ nm

expectation of a possible designing of QW nitride devices manufactured on the InP substrate and emitting radiation of much longer wavelengths than those manufactured on the GaAs substrate.

## 5 Conclusions

In the present paper, possibility of designing long-wavelength (≥2.0 μm) InP-based quantum-well (QW) GaInNAs diode lasers is considered with the aid of the comprehensive computer simulation. This emission may be widely applied in a distant air monitoring, laser spectroscopy, medical diagnostics, thermovision measurements, and wireless optical communication, to name the most important areas of its application. It is well known that such a long-wavelength emission by the GaAs-based QW diode lasers is impossible. However, potential emission properties of similar InP-based diode lasers seem to be very promising, although they are still not fully discovered. Therefore, their anticipated performance characteristics are determined in the present paper with the aid of our comprehensive computer model. In the simulation, both the QW material and intentionally introduced stresses have been carefully selected to determine optimal diode-laser structure for an efficient emission of the above long-wavelength radiation at room temperature. It is evident from our analysis that the compressively strained InP-based $Ga_{0.12}In_{0.88}N_{0.02}As_{0.98}/Ga_{0.275}In_{0.725}As_{0.6}P_{0.4}$ QW structure has been found to offer expected anticipated lasing emission. For its QW thickness of 10 nm and the carrier concentration of $5 \times 10^{18}$ cm$^{-3}$, its maximal optical gain of over 2150 cm$^{-1}$ is at room temperature shifted as much as to about 2815 nm (Fig. 6c). Therefore, similar QW structures may be successfully applied in compact semiconductor laser sources of the desired radiation of wavelengths longer at room temperature than even 2800 nm, which is much greater than their values in GaAs-based similar devices. Possible further wavelength increase requires further investigations.

**Acknowledgements** This work has been supported by the Polish Ministry of Science and Higher Education (MNiSzW), grant No. N N515 533338 and by the COST Action MP0805.

**Open Access** This article is distributed under the terms of the Creative Commons Attribution License which permits any use, distribution, and reproduction in any medium, provided the original author(s) and the source are credited.

## References

1. Z. Yin, X. Tang, Solid-State Electron. **51**, 6 (2007)
2. W. Both, A.E. Bochkarev, A.E. Drakin, B.N. Sverdlov, Cryst. Res. Technol. **24**, K161 (1989)
3. M. Guden, J. Piprek, Model. Simul. Mater. Sci. Eng. **4**, 349 (1996)
4. G. Almuneau, E. Hall, T. Mukaihara, S. Nakagawa, C. Luo, D.R. Clarke, L.A. Coldren, IEEE Photonics Technol. Lett. **12**, 1322 (2000)
5. T. Borca-Tasciuc, D.W. Song, J.R. Meyer, I. Vurgaftman, M.-J. Yang, B.Z. Nosho, L.J. Whitman, H. Lee, U. Martinelli, G.W. Turner, M.J. Manfra, G. Chen, J. Appl. Phys. **92**, 4994 (2002)

6. T. Newell, X. Wu, A.L. Gray, S. Dorato, H. Lee, L.F. Lester, IEEE Photonics Technol. Lett. **11**, 30 (1999)
7. L. Shterengas, G.L. Belenky, J.G. Kim, R.U. Martinelli, Semicond. Sci. Technol. **19**, 655 (2004)
8. S. Abdollahi Pour, B.-M. Nguyen, S. Bogdanov, E.K. Huang, M. Razeghi, Appl. Phys. Lett. **95**, 173505 (2009)
9. H.-P.D. Yang, C. Lu, R. Hsiao, C. Chiou, C. Lee, C. Huang, H. Yu, C. Wang, K. Lin, N.A. Maleev, A.R. Kovsh, C. Sung, C. Lai, J. Wang, J. Chen, T. Lee, J.Y. Chi, Semicond. Sci. Technol. **20**, 834 (2005)
10. I. Vurgaftman, J.R. Meyer, L.R. Ram-Mohan, J. Appl. Phys. **89**, 5815 (2001)
11. I. Vurgaftman, J.R. Meyer, J. Appl. Phys. **94**, 3675 (2003)
12. S. Wang, Phys. Status Solidi, B Basic Res. **246**, 1618 (2009)
13. S. Adachi, *Properties of Semiconductor Alloys: Group-IV, III-V and II-VI Semiconductors* (Wiley, Chichester, 2009)
14. Y.P. Varshni, Physica **34**, 149 (1967)
15. R. Kudrawiec, J. Appl. Phys. **101**, 023522 (2007)
16. L.F. Xu, D. Patel, C.S. Menoni, J.Y. Yeh, L.J. Mawst, N. Tansu, Appl. Phys. Lett. **89**, 171112 (2006)
17. Z. Pan, L.H. Li, Y.W. Lin, B.Q. Sun, D.S. Jiang, W.K. Ge, Appl. Phys. Lett. **78**, 2217 (2001)
18. M. Hetterich, M.D. Dawson, A.Yu. Egorov, D. Bernklau, H. Riechert, Appl. Phys. Lett. **76**, 1030 (2000)
19. J.B. Héroux, X. Yang, W.I. Wang, J. Appl. Phys. **92**, 4361 (2002)
20. M.H. Gass, A.J. Papworth, T.B. Joyce, T.J. Bullough, P.R. Chalker, Appl. Phys. Lett. **84**, 1453 (2004)
21. J.-Y. Duboz, J.A. Gupta, M. Byloss, G.C. Aers, H.C. Liu, Z.R. Wasilewski, Appl. Phys. Lett. **81**, 1836 (2002)
22. G. Baldassarri Höger von Högersthal, A. Polimeni, F. Masia, M. Bissiri, M. Capizzi, D. Gollub, M. Fischer, A. Forchel, Phys. Rev. B **67**, 233304 (2003)
23. T. Ikari, K. Imai, A. Ito, M. Kondow, Appl. Phys. Lett. **82**, 3302 (2003)
24. A. Polimeni, F. Masia, G. Baldassarri Höger von Högersthal, M. Capizzi, Chap. 7, in *Dilute Nitride Semiconductors*, ed. by M. Henini (Elsevier, Oxford, 2005)
25. D.-K. Shih, H.-H. Lin, L.-W. Song, T.-Y. Chun, T.-R. Yang, in *Proceedings of the 13th International Conference on Indium Phosphide and Related Materials*, Nara, Japan, 14–18 May 2001 (2001), p. 555
26. W.K. Hung, K.S. Cho, M.Y. Chern, Y.F. Chen, D.K. Shih, H.H. Lin, C.C. Lu, T.R. Yang, Appl. Phys. Lett. **80**, 796 (2002)
27. D.R. Hang, D.K. Shih, C.F. Huang, W.K. Hung, Y.H. Chang, Y.F. Chen, H.H. Lin, Physica E **22**, 308 (2004)
28. T.H. Glisson, J.R. Hauser, M.A. Littlejohn, C.K. Williams, J. Electron. Mater. **7**, 1 (1978)
29. W. Shan, W. Walukiewicz, J.W. Ager III, E.E. Haller, J.F. Geisz, D.J. Friedman, J.M. Olson, S.R. Kurtz, Phys. Rev. Lett. **82**, 1221 (1999)
30. G.E. Pikus, G.L. Bir, Sov. Phys., Solid State **1**, 1502 (1960)
31. G.L. Bir, G.E. Pikus, *Symmetry and Strain-Induced Effects in Semiconductors* (Wiley, New York, 1974)
32. S.L. Chuang, *Physics of Optoelectronic Devices* (Wiley, Chichester, 1995)
33. P.G. Eliseev, Electron. Lett. **33**, 2046 (1997)